IEEE Robotics and Automation Letters (RAL) paper presented at the
2020 IEEE/RSJ International Conference on Intelligent Robots and Systems (IROS)
October 25-29, 2020, Las Vegas, NV, USA (Virtual)

Energetic Passivity Decoding of Human Hip Joint for Physical Human-Robot Interaction

S. Farokh Atashzar*,[1], Hsien-Yung Huang*,[2], Fulvia Del Duca[3], Etienne Burdet[2], Dario Farina[2]

***Abstract*— The capacity of the biomechanics of human limbs to absorb energy during physical human-robot interaction (pHRI) can play an imperative role in controlling the performance of human-centered robotics systems. Using the concept of "excess of passivity", we have recently designed passivity signature maps for elbow and wrist joints. We have also shown that this knowledge can be exploited and extrapolated during the interaction with a robotic system by transparency-maximized algorithms. A major application is in robotic rehabilitation systems and assistive technologies. Here, for the first time, the nonlinear energy capacitance of the hip joint and the affecting factors are decoded. This can be critical for maximizing the performance of wearable exoskeletons. Knowledge regarding energy absorption behavior can significantly help to reduce the conservatism of control algorithms. In this work, the energetic behavior is studied for three different hip angles, while perturbations were provided at three different interaction speeds. The results show that the increase in agonist and antagonist muscle contractions can consistently expand the margins of the passivity map. Additionally, by separating the effects of agonist and antagonist contractions, it was identified that the passivity margins have a correlation with the subject's posture during interaction with the robot and the correlation depends on the type of muscle contraction. A preliminary design of a stabilizer is also formulated that takes into account variable passivity behavior of the joint, in the energy domain, to enhance the performance while guaranteeing pHRI stability.**

I. Introduction

Human-centered robotics (HcR) systems have shown great potential to enhance human sensorimotor capability. The technology has been used for reaching beyond the natural competence of humans and for relaxing physiological and pathological barriers [1]. HcR technology has also been used for studying human sensorimotor function and the corresponding learning-based characteristics [2], [3], [4], [5]. Examples of HcR systems are rehabilitation robotic modules and rehabilitative exoskeletons [1], [6], [7]. Medical HcR (M-HcR) technology for rehabilitation (in particular for upper-limb rehabilitation) comprises robotic systems that are connected to the patients' body to generate and deliver assistive (and in some cases resistive) force fields while the patient performs tasks in a virtual reality environment. Arguably, the quality of the force field is critical for realizing an efficient therapeutic regimen. Force fields are designed to promote active participation and maximizing engagement [8], [9]. To achieve this goal, robotic systems should respond promptly to the patient's voluntary motions [10], [11] while inhibiting involuntary actions [12], [13], [14], [15], [16]. This imposes the need for a large bandwidth for the response to voluntary actions. The technical challenge is that realizing a high bandwidth of kinesthetic assistance can increase the possibility of approaching instability for human robot interaction. This is caused by the fact that the assistive behavior of robotic systems does not follow conventional (and conservative) energy passivity assumptions. Based on the weak passivity theorem [17], [18], [19] from nonlinear control theory, a cascade interconnected system (the output of one subsystem activates the input of the other subsystem and vice versa) remains stable if the two subsystems (e.g. human biomechanics and robotic force field) are passive. A system with input vector $x(t)$, output vector $y(t)$, and initial energy β_0 is passive [18], [19], [20], [21], [22] if there exists a constant β_0 such that for all $t \geq 0$

$$\int_0^t x(\tau)^T \cdot y(\tau)\, d\tau \geq \beta_0. \tag{1}$$

Conventionally the operator's limb is assumed to be passive, considering force-velocity coupling [20], [23], [24]. The weak passivity theorem has been used for dynamic analysis of haptics-enabled telerobotics systems and haptics rendering technology in which one terminal (subsystem) is the human biomechanics, and one terminal is the simulated (or remote) environment which generates the repulsive force field, and on which the actions of the user are applied. In many cases, for example, in haptics-simulators or haptics-enabled telerobotic systems, the environment has been assumed to be passive and often modeled using passive linear dynamics (e.g., mass-spring-damper models) [25], [26].

The communication and digitization time delays can result in the non-passive behavior of a terminal [23], [25], [27], [28]. Time delays can result in the accumulation

This study was supported in part by European Commission under grant H2020-ICT-23-2017-779982 EXTEND, and by grant H2020 ICT 871767 REHYB, and in part by National Science Foundation Award Number: 2031594.

* Atashzar and Huang share the first authorship.

[1]Atashzar (corresponding author) is with the Department of Mechanical and Aerospace Engineering and Electrical and Computer Engineering, New York University (NYU), USA. Atashzar is also with NYU WIRELESS. f.atashzar@nyu.edu

[2]Huang, Burdet, and Farina are with the Department of Bioengineering, Imperial College London, UK.

[3]Del Duca is with the Department of Electrical and Computer Engineering, Technical University of Munich, Germany.

of energy in closed-loop systems during the interaction, which can violate the passivity assumption and result in instability and exponential growth of force and velocity. Such a situation, during human-robot interaction, is a serious safety concern and can result in soft tissue injuries and bone fractions [29].

Several techniques and controllers have been proposed to stabilize the behavior of interconnected systems that include time delay, e.g. [25], [28], [30], [31], [32], [33], [34]. In this regard, passivity-based controllers, such as energy-based and power-based time-domain passivity approaches (TDPA) [28], [30], [31], [32], inject an adaptive damping factor to dissipate energy and guarantee the passivity of the interconnected system based on the weak passivity theorem (1). The performance of these techniques has been supported in several papers including our publications [33], [35]. On the other hand, wave variables controllers [19], [25], [36], [37] assume passivity of the terminals and strictly focus on making the two-port communication network passive (applied for telerobotics systems).

Although there exist several controllers and algorithms to stabilize a non-passive interconnection of subsystems with communication delay, in assistive technologies, the therapy terminal is not (and cannot be converted to) a passive component, since the programmed virtual therapist has to inject energy in order to assist movements [34]. As a result, implementing classical derivations of controllers, such as TDPA, for assistive therapies will result in excessively dampening of the assistance and compensating for the assistive power generated by the robot [33], [34], [35].

II. Preliminaries

It should be highlighted that the assistive force field is indeed the critical factor needed to realize transparent robotic assistance and dampening it is counterproductive. As a result, the classical design of controllers cannot be directly applied to guarantee the safety and stability of assistive HcR technologies. This has resulted in conservative precautions in the design of controllers, including limiting the reactive behavior of assistive robots, along with the assistive gains, force, velocity, and acceleration profiles. The aforementioned limitations have saturated the expected performance and potential benefits of the technology for many patients, such as those who require high amplitude forces to embrace assisted rehabilitative exercises, those with hypertonia (a common stroke symptom), and those with heavy biomechanics. A direct consequence is that, despite significant advances in the mechatronic design of rehabilitative robots and exoskeletons, users cannot take the full advantage of a potentially agile and transparent assistive force field produced using a robotic rehabilitation system and exoskeletons.

We have recently investigated this issue and have confirmed that the nonpassive assistive behavior of robotic systems could indeed result in energy accumulation and instability, *if and only if a particular computational stability condition is violated* [33], [35]. We have shown that the stability condition of an assistive system depends on the "extent" of the passivity of the user's biomechanics and the "aggressiveness" of the nonpassive assistive force field. Taking advantage of the strong passivity theorem, we have shown that if the excess of the passivity (EoP) of the limb biomechanics is larger than the shortage of passivity (SoP) of the assistive force field, the system remains stable regardless of the absolute nonpassive behavior [33], [35] (definitions of excess and shortage of passivity are given below). However, if the user's biomechanics does not guarantee sufficient EoP and/or if the assistive force field is highly nonpassive (have a high SoP), the interconnection of the two subsystems will tend to be unstable. In this case, we have recently proposed novel stabilizing algorithms that minimize the needed compensation considering the difference between energy absorption capacity and the delivered energy [33], [35]. Mathematical definitions of EoP and SoP are as follows.

For the system introduced in (1), if there is a constant β_0 such that for all $t \geq 0$ we have

$$\int_0^t x(\tau)^T \cdot y(\tau)\, d\tau \geq \beta_0 + \delta \cdot \int_0^t x(\tau)^T \cdot x(\tau)\, d\tau, \quad (2)$$

and if $\delta \geq 0$, the system is Input Strictly Passive (ISP) and the EoP is δ. However, if $\delta < 0$, the system is Input Non-Passive (INP) and the SoP is δ [18], [21], [22].

In addition, for the same system if we have

$$\int_0^t x(\tau)^T \cdot y(\tau)\, d\tau \geq \beta_0 + \xi \cdot \int_0^t y(\tau)^T \cdot y(\tau)\, d\tau, \quad (3)$$

for $\xi \geq 0$, the system is Output Strictly Passive (OSP) and the EoP is ξ. If $\xi < 0$, the system is Output Non-Passive (ONP) and the SoP is ξ [18], [21], [22].

As a result, a HcR system with an INP assistive force field (nonpassive therapeutic terminal) can still remain L_2 stable if the energy generated by the assistive force field is smaller than the energy which can be absorbed by the impeding OSP component of the patient's limb. To guarantee this stability condition, the EoP of the patient's biomechanics should be larger than the SoP of the therapy terminal.

Motivated by the above-given notion, we have recently conducted a user study to evaluate the passivity of the wrist and elbow joint. The focus was to investigate how the passivity of the wrist and elbow reactive dynamics changes during different levels of co-contraction and if this information can be used in the design of a nonlinear control system that can take into account the patient's EoP and changes in the corresponding EoP to enhance the stability of HcR systems while minimizing the conservatism. Thus, a control framework was formulated to monitor the energy capacity of the user's biomechanics in real time and modify the

reflected interactive energy, enough to guarantee the safety while avoiding excessive damping of the assistive energy, to maximize realizable transparency [33]. The framework allows for achieving a unique performance of HcR systems, by modifying the corresponding stabilizing behavior based on the user-specific energy signature.

In the literature, the passivity behavior of biomechanics has been also studied using other techniques for the ankle joint [38]. In [38], it is shown that the ankle joint represents a predominant dissipative behavior in young, healthy subjects, which can be potentially used as a "quantitative knowledge of human interactive dynamics" for realizing a "less conservative design" of control systems.

This paper evaluates the passivity signature of the hip joint while considering the effect of the hip rotation angle through three interaction velocities. This allows us to generate an energy signature map of the hip joints of two subjects participating in this study, and to enable predicting the energy absorption capacity during human-robot interaction. For this purpose, we have utilized a particular design of a perturbation system to collect the interactive profiles and compute the signature map. Due to the complexity of the hip joint biomechanics and the corresponding significant role in gait, we also evaluated the passivity behavior in different joint angles to understand whether this information (potential dependency on the angle) should be incorporated in the design of a controller which takes into account the energy behavior of the hip joint (see the appendix). For this, at each joint angle, we applied limb perturbations with three velocities, which is critical considering the large variation of hip velocity during different paces of gait. It should be noted that the mathematical foundation for the current study does not assume any linearity in the energetic behavior of the hip joint.

III. Methods

A. Experimental Setup

In order to calculate the EoP of the hip joint, force and velocity information should be collected during several iterations of an identification trial. For this purpose, we used the dedicated Neuromechanics Evaluation Device (NED) that we have recently developed (please see Fig.1, and [39], [40] for more details). NED is a versatile robotic interface that enables controlled leg position perturbations while the subject is seated and maintained in an upright posture. A locking knee brace was used to maintain the knee joint straight throughout the experiment to isolate the hip joint biomechanics for the study. The motor, which is securely bolted to the floor, will apply controlled motions to the leg just above the ankle joint via the steel cable loop and the ankle fixture. During the experiment, the robotic interface will record the interaction force (using two load-cells located on both sides of the ankle fixture and connected to the cables), in addition to hip angle and rotational velocity,

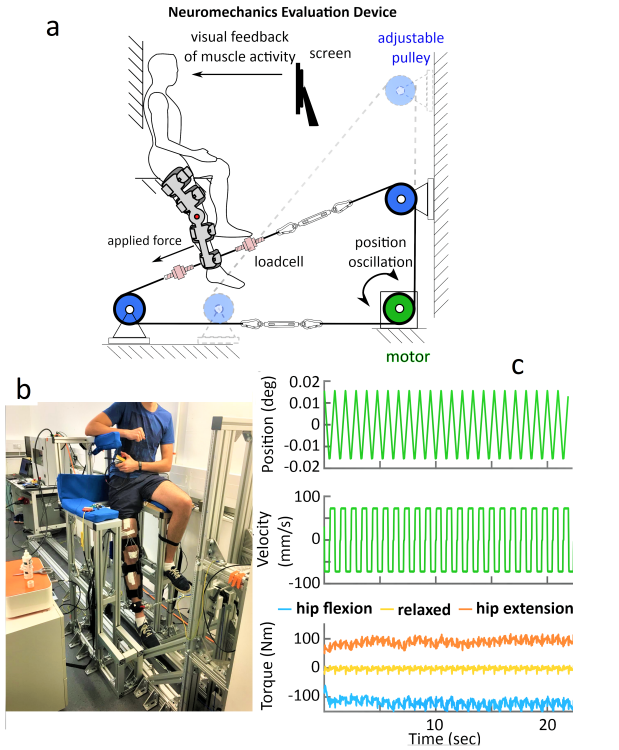

Fig. 1. Sketch of the Neuromechanics Evaluation Device (NED) and sample measurements. (a, b) the experiment setup. Visual feedback is provided to the subjects based on their muscle activities and interactive forces. While the subject tunes the interactive forces, NED provides position-domain oscillatory perturbations. (c) A sample of position, velocity, and torque recording.

and muscle activity (through electromyography recordings) simultaneously. The pulley mechanism of the NED system is adjustable to the participant's leg length, and also to the desired experiment hip angle. This allows the robot to exert accurate normal force, also enabling accurate evaluation of the energy signature of the joint at different angles. The developed interface includes various safety features to track and protect the participant's safety throughout the experiment. This includes software limitations (velocity, acceleration and jerk), optical systems to define the maximum leg displacement and emergency buttons for both the participant and the experimenters.

B. Experiment Design

The experimental protocol was approved by the Imperial College Research Ethics Committee. Two healthy subjects without known history of neurological or musculoskeletal injury were recruited, who were informed about the robotic interface and experimental procedure, and provided a signed consent prior to participating. Demographic subjects data are provided in Table I. The leg length was measured from the anterior superior iliac spine to the lateral malleolus.

Bipolar electromyography (EMG) electrodes were positioned on the Rectus Femoris (RF) and Biceps Femoris

(BF) muscles. The EMG electrodes were connected to a signal amplifier (EMG-USB2+, OT Bioelettronica) to monitor muscle activation. EMG signals were baseline corrected, filtered with a [5,500]Hz bandpass 2nd order Butterworth filter, rectified, and processed for extraction of the envelope. A locking knee brace was used to maintain the knee joint straight throughout the experiment (Fig.1), and to isolate the hip joint biomechanics for the study. The participants were asked to sit in the NED system with the leg relaxed while supporting their body weight using the handle (Fig.1). A harness was placed around the ankle, and was connected to the cable-driven perturbation system providing the oscillatory motions for identification. To calibrate the safety, the software limitations and optical safety system were tuned while the subject's leg was slowly moved around the allowable workspace. An emergency button was always within the subject's reach in case of discomfort.

TABLE I

BIOGRAPHICAL INFORMATION OF THE SUBJECTS

no	weight [kg]	height [m]	leg length [m]	age	sex
1	71	1.81	0.97	24	M
2	70	1.74	0.92	24	M

C. Maximum Voluntary Contraction (MVC) Phase

Each experiment cycle at a given hip angle started with an MVC test to benchmark the maximum force and EMG values at the tested posture. The participant was verbally encouraged to pull the cable with the maximum comfortable leg strength for approximately three seconds. Then ten seconds of rest were given, and the MVC test was conducted again. This sequence was repeated twice for both flexion and extension of the hip joint. The maximum EMG magnitude of both muscle groups was then used to define the 15% MVC level for conducting the rest of the experiment.

D. Posture Perturbation Phase

After the MVC test and a five minute break, for one chosen hip angle, the subject was randomly assigned to one of the following tests: relax, leg flexion (with a 15% MVC muscle contraction level), and leg extension (with a 15% MVC muscle contraction level). The participant controlled the EMG activity based on the provided visualization of the commanded target and realtime feedback. The cable-driven system then provided a cyclic leg displacement at a specified speed for 2 min. Measurement was repeated at three speeds 70, 150, 230 mm/s, and in combination with three muscle contraction levels relaxed, flexion 15% MVC, extension 15% MVC. After testing the above-mentioned 9 combinations of tests, the participant was given a ten minute rest, and then the same protocol was repeated for another hip angle. The three tested initial angles were $\{15°,35°,55°\}$. EMG data collection was at 2048 Hz, and the force and kinematics were measured at 1000 Hz.

E. Data analysis and EoP Estimation Phase

Given the definition of EoP in the OSP model of reactive dynamics (3), the general equation to estimate the EoP of the hip (at a given condition of hip joint angle of θ, muscle contraction level of i, and perturbation speed of s) is:

$$\xi_{\theta,i,s} = \int_{Ts}^{Te} \frac{\tau^T(t)\cdot\omega(t)}{\omega^T(t)\cdot\omega(t)}dt. \tag{4}$$

In (4), $\xi_{\theta,i,s}$ is the identified EoP value at the respective conditions (θ, i and s), τ the interaction torque, ω the hip joint angular velocity, T_s and T_e the start and ending time of the oscillation stimulation. The linear displacement velocity measured by sensors was converted to the angular velocity of the hip joint (ω). Also, the interaction torque (τ) measured at the ankle was calculated from the difference between the force measurements of two load-cells placed on both sides of the ankle fixture.

In order to extract the EoP, we should isolate the reactive and active components of dynamics and force generation by the user during interaction with the robot [33]. The reactive component, which is responsible for absorbing mechanical energy during the interaction, is part of the dynamics that results in impeding force regardless of the direction of interaction. It is generated in response to the external perturbation and plays a critical role in the stability condition of the interaction between human and robot. However, the active component of force, which results in targeting and motion, is mainly generated voluntarily to promote/ initiate/ continue motion in a particular direction and should be treated as an external input to the system (in the context of strong passivity theory). The active dynamical component does not affect the closed-loop behavior of the system and energy absorption capacity. This isolation of the reactive dynamics is straightforward when working on upper limb due to the simpler actions of biomechanics. In our previous work which was conducted on the upper-limb energy behavior, we have isolated the reactive component by asking the participants not to initiate motions during perturbation and to allow the robot to perturb their limb while they generated various levels of co-contraction through various grasping levels. The corresponding co-contraction changes the impeding behavior of the biomechanics, which modulates the reactive dynamics. This, however, is not as straightforward for the hip joint, since voluntary co-contraction of muscles activating the hip is not intuitive for all. As a result, a different protocol was needed to assess the capacity of energy absorption of the hip joint and the changes in the impeding reactive dynamics by flexion and extension of the joint.

In this study, to generate different levels of consistent muscle activation, while studying the nonlinear and asymmetric impeding energetic behavior, we have asked the subjects to keep a particular flexion/extension level of force and muscle activation, while the robot perturbed their limb.

For this, participants were asked to "push" at an instructed direction in order to activate different hip muscle groups. This was intuitive for participants. During this period, we collected data to evaluate the corresponding effect of the particular muscle contraction on the energetic behavior of the joint.

As a result, to isolate reactive and active dynamics, in the calculation, we extracted and evaluated parts of data that were related to the impeding/opposing periods during which the contraction generated by the user opposes the direction of perturbation. During the mentioned periods of time, the reactive component plays the major role in the interaction dynamics. However, during the period in which the robot skips away from the user's current position (which means that the motion of the robot and the user are in the same direction), the interactive dynamics is more activated by its active (not reactive) component since the user should also execute controlled motion for keeping the prescribed flexion or extension level. In order to incorporate this into the calculation, Eq. (4) was modified as follows:

$$\xi_{\theta,i,s} = \int_{Ts}^{Te} \frac{\tau^T(t)\cdot\omega(t)}{\omega^T(t)\cdot\omega(t)} \cdot Z(t)dt \qquad (5)$$

In (5), $Z(t)$ is an additional imposed condition that turns the integral on and off during the cycle of perturbation for proper calculation of EoP, depending on the contraction state, and to isolate active and reactive components of dynamics. The $Z(t)$ condition is imposed with considering the relationship between the direction of displacement $p_{\theta,i,s}(t)$ and the direction of contraction $k_{p_{\theta,i,s}}(t)$, at each time instant t as given below.

$$Z(t) = \begin{cases} 1, & \text{if } p_{\theta,i,s}(t) \neq k_{p_{\theta,i,s}} \\ 1, & \forall t \text{ if } k_{p_{\theta,i,s}} = 2 \\ 0, & \text{otherwise.} \end{cases} \qquad (6)$$

where $k_{p_{\theta,i,s}}$ is an integer number indicating the leg contraction direction, where $k = 1$ during muscle flexion state, $k = -1$ during extension state and $k = 2$ during relaxed state. Also $p_{\theta,i,s}(t)$ is an integer which is equal to 1 if the leg is displaced by the robot into hip flexion, and is -1 if the leg is displaced into hip extension. In other words, the imposed condition $Z(t)$ allows us to compare the direction of contraction and direction of motion to activate the integral in a way that extracts the component of interaction which is mainly influenced by reactive component of dynamics.

To analyze the results, data from all three speeds were concatenated at each condition {hip angle and contraction level}, and the concatenated data was used to estimate the EoP, this time not for one single perturbation velocity but for a larger range of perturbation frequencies.

IV. Results

Fig.2 shows representative EMG recordings measured at different contraction levels. As expected, in most experiments both subjects were able to follow the target muscle activation level. Additionally, the average antagonist muscle contraction levels were lower than 5% MVC value, which indicates the subjects' consistency in independent control of flexion versus extension during the course of the experiment. The average agonist contraction and the antagonist opposite-contraction levels of all subjects of different experiment conditions are listed in Table.II. In an ideal case the targeted muscle contraction level should be 15% and the opposite muscle contraction level should be 0%. The results in Table.II show a good agreement with this ideal case.

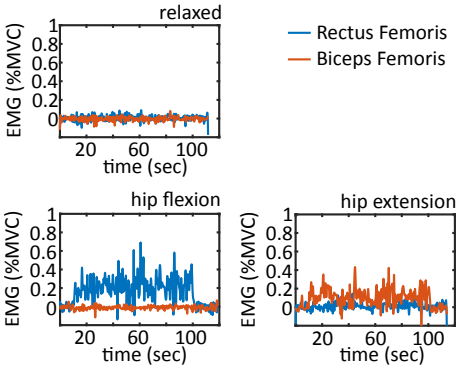

Fig. 2. Sample EMG recording. The muscle activities at the relaxed condition show a low contraction, while both at the hip flexion and extension cases they oscillate around the targeted contraction at respective muscle groups.

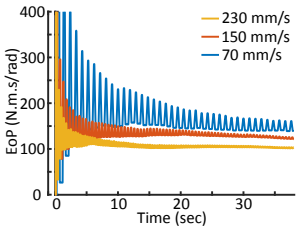

Fig. 3. Sample EoP measured at three different speeds.

TABLE II
AVERAGE MUSCLE CONTRACTION LEVELS

subject	angle	contraction direction	targeted muscle contraction (%MVC)	opposite muscle contraction level (%MVC)
1	55	forward	9	2
1	55	backward	37	2
1	35	forward	8	2
1	35	backward	13	5
1	15	forward	13	0.8
1	15	backward	14	0.7
2	55	forward	17	0.6
2	55	backward	14	5
2	35	forward	17	2
2	35	backward	15	2
2	15	forward	13	0.4
2	15	backward	22	4

Fig.3 shows an example of estimated EoP during the three different perturbation speeds, before concatenating the corresponding data. As can be seen in the figure, the EoP

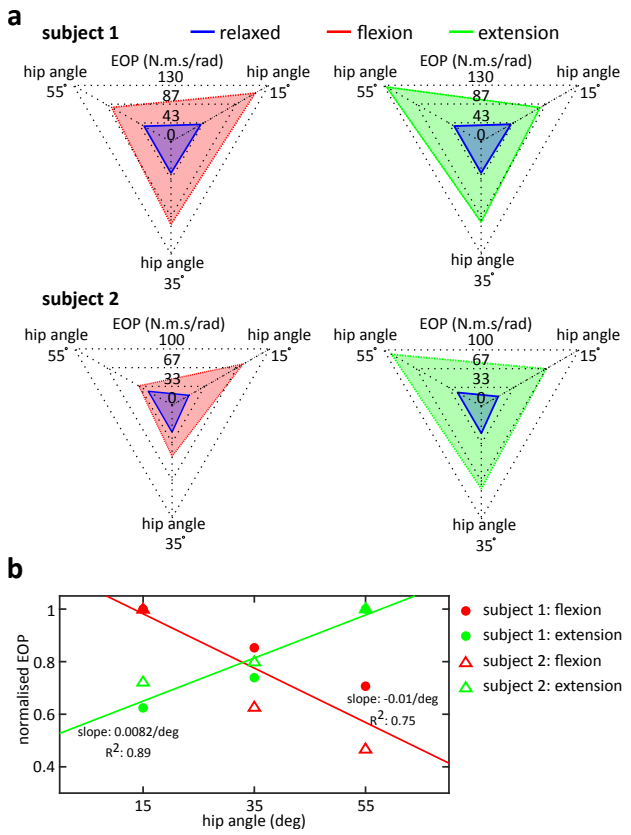

Fig. 4. Panel (a) shows the estimated EOP values of both subjects at different contraction level and hip angle. The distance from the center to the corners of the triangular radar plot indicates the magnitude of the estimated EOP values. Each corner of the radar plots represents the estimation at a different hip angle. The color blue shows the EOP values identified in the relaxed condition, while the hip flexion and extension are represented by red and green, respectively. Panel (b) shows the posture dependency of the EOP values. By linear regressing the estimated EOP values, it is found that the EoP value increases with posture while performing hip extension (with a slope of 0.0082/deg, R^2 = 0.89) and decrease when conducting hip flexion (with a slope of -0.01/deg, R^2=0.75).

value may also change depending on the perturbation speeds and frequencies. In order to estimate the most representative energetic behavior, we utilize the concatenating approach for the three perturbation speeds to enhance the richness of information for the estimation process. Fig.4 illustrates the estimated EOP values of both subjects at different postures and different contraction levels and at different perturbation angles, after concatenating the data. The estimated EoP values related to both flexion and extension are compared individually with the relaxed condition using a radar plot (Fig.4a). It is shown that both leg flexion and extension resulted in a significant increase in the EoP value in all posture angles, in comparison to the relaxed condition. Additionally, after normalization (Fig.4b), the EoP values are found to correlate with changes in the hip posture. By linear regressing the estimated EOP values, it is found that the EOP value increases with posture while performing hip extension (with a slope of 0.0082/deg, R^2 = 0.89) and decrease when conducting hip flexion (with a slope of -0.01/deg, R^2=0.75). In the case of a forward contraction (flexion), the highest EoP was found at 15° hip angle and the lowest EoP is observed at 55° hip angle. Inversely, the backward contraction (extension) resulted in a highest EoP value at the hip angle 55° and the lowest value at 15°.

Results above show that the energy absorption ability of the hip joint consistently changes by muscle contractions, geometry and posture of interaction. The aforementioned dependencies can be computationally identified and modeled using energetic passivity maps. The results show that the passivity maps are (a) asymmetric (varies in different directions and posture), (b) muscle group dependent, (c) posture-dependent, and (d) user-dependent. Indeed, the radar plots show the "signature" of the hip joint in terms of the absorption capacity for interactive energy.

The map may be directly used to assess changes in dynamical behavior of the joint biomechanics with respect to energy absorption ability. In addition, identifying the map and then extrapolating it during interaction with a robotic system (based on the measured contraction level, type of contracted muscle, current posture, and the direction of contraction) can allow an intelligent controller/stabilizer to provide the minimum needed damping for stabilizing the system. In other words, the controller of the robot can adaptively tune the stabilizing behavior (which defines the performance and system transparency) based on the current states of the interaction (mentioned above) and the pre-identified knowledge of the hip joint regarding the energetic passivity behavior. Thus, the stabilizer (see the appendix) can take advantage of energy reservoirs in human biomechanics to minimize performance distortion and maximize transparency. Thus, if a user shows a significant increase in the energy absorption ability at one specific direction, one specific muscle contraction level and type, the controller will not distort the delivered assistive energy.

V. Conclusion

This paper evaluates the energy absorption capacity of the human hip joint during interaction with robotic systems. The outcome is critical for wearable robotic technologies, including exoskeletons. In this paper, for the first time, we have decoded the energetic signature of the human hip and have shown if and how it changes based on muscle contraction, depending on muscle groups, direction, and posture of interactions. The results show a consistent energetic behavior of hip with respect to the posture of perturbation. The results also show that the EoP can significantly change by increasing muscle contraction and that the change is asymmetric depending on the direction of interaction, posture, and muscle group. These results can be directly used to (a) design a nonlinear controller ensuring "minimal stability" based on strong passivity control theory

(see Appendix) and (b) to design a representative atlas of energy signature maps of the hip joint by collecting data from more participants, to allow for predicting the passivity behavior, based on minimum available knowledge. In this paper, the result of experimental validation on two participants is provided. A clinical direction of the future work of this study will be focused on the evaluation of the passivity-based signature of human biomechanics (in particular the hip joint) for a larger population, as a new tool to objectively characterize the lower-limb neuromechanical impairments caused by neurological diseases and musculoskeletal disorders.

VI. Appendix: Energy Domain Stability Using a Variable Structure Passivity Controller

In this Appendix, we provide a new design of a nonlinear controller, which can guarantee the stability of physical human-robot interaction using variable excess of the passivity of the limb and can be used in various robotic interfaces. The particular design allows for incorporating the "variability of EoP" in the design of the variable structure controller. As explained earlier, there are several factors (contraction level of different muscle groups, the direction of interaction, posture angle) that result in the variation of EoP of the hip joint. Measuring those factors, we can estimate the EoP in realtime. In this Appendix, we answer this question: "how the estimated EoP can be encoded in the design of a nonlinear controller that can utilize the knowledge on EoP."

The theoretical developments are based on our recent work [33] for the upper limb, in which we have designed a power-domain stabilizer considering the grasp condition. Such a stabilizer may be conservative, in general, since it does not consider the energetic history of interaction and aim for guaranteeing passivity at the power level. This can result in excessive modification of the reflected force during human-robot interaction since any non-positive power packet will be treated as a potential source of instability. However, to guarantee the passivity, the integral should be positive. In other words, although the positiveness of every interactional power packet is a sufficient condition for the positiveness of the corresponding integral (energy of interaction), this is not a necessary condition. In this appendix, our recently designed power-domain stabilization [33] is modified to take into account the passivity behavior of the biomechanics in the energy domain. In [33] we have shown that for physical human-robot interaction, the interconnected system will be passive (and thus stable) if the following condition is held.

$$\int_0^t f_{react}(\tau)^T \cdot v_p(\tau) + f_p(\tau)^T \cdot v_p(\tau)\, d\tau \geq 0. \quad (7)$$

In (7), f_{react} is the reactive response (force/torque) of the user's biomechanics, v_p is the velocity of the user's limb, and f_p is the therapeutic force to be delivered to the patient's limb (for assistance or rehabilitation). In the presence of a stabilizer which adaptively modulates the reflected forces to the patient's limb, the new stability condition is as follows, in which f_{p-mod} is the modified reflected force.

$$\int_0^t f_{react}(\tau)^T \cdot v_p(\tau) + f_{p-mod}(\tau)^T \cdot v_p(\tau)\, d\tau \geq 0. \quad (8)$$

The above stability condition can be rewritten as

$$E_{p-react}(t) \geq -E_{p-mod}(t). \quad (9)$$

In (9), $E_{p-react} = \int_0^t f_{react}(\tau)^T \cdot v_p(\tau)\, d\tau$ is the energy that can be absorbed by the biomechanics of the patient's limb, while $E_{p-mod}(t) = \int_0^t f_{p-mod}(\tau)^T \cdot v_p(\tau)\, d\tau$ is the therapeutic energy delivered to the patient's limb after the modification (explained below) by the nonlinear stabilizer.

In order to design the stabilizer, the question is how to induce the modification into f_p to satisfy the given passivity condition. For this, the main challenge is that f_{react} would be needed. However, f_{react} is neither accessible nor measurable because the measurable force is mixed with the voluntary exogenous force generated by the user's muscles for producing motion. This has been shown in the literature [35], [33] by decomposing the human force into exogenous component $f_p^*(t)$ and reactive component of the biomechanics, $f_{react}(t)$, as shown in (10) (details can be found in [33]):

$$f_p(t) = f_p^*(t) - f_{react}(t), \quad \text{where} \quad f_{react} = z_p(v_p, t) \quad (10)$$

In (10) $z_p(v_p, t)$ is the generalized nonlinear impedance model of the reactive dynamics of the user's biomechanics. Thus a force/torque sensor at the interaction point during human-robot interactions can measure $f_p(t)$. However, $f_{react}(t)$ is needed for calculating $\int_0^t f_{react}(\tau)^T v_p(\tau)\, d\tau$ to be used in a power modification or energy modification scheme through force modulation for guaranteeing passivity. The answer is the use of excess of passivity in realtime considering the corresponding variability as discussed. This is to estimate and utilize a variable lower bound for the amount of energy which can be absorbed by the user biomechanics during interaction, i.e., $\int_0^t \xi_p(\tau) v_p(\tau)^T v_p(\tau) d\tau$. The proposed controller will work as follows:

$$f_{p-mod}(t) = \begin{cases} f_p(t) & \text{if } \int_0^t f_\tau(t)^T \cdot v_p(\tau)\, d\tau \geq 0, \\ \Psi(t) & \text{otherwise.} \end{cases} \quad (11)$$

In (11), we have

$$\Psi(t) = \begin{cases} f_p(t) \;\; \text{if } \int_0^t \xi_p(\tau) v_p(\tau)^T v_p(\tau)\, d\tau \geq \\ \qquad\qquad -\int_0^t f_p(\tau)^T \cdot v_p(\tau)\, d\tau, \\ ||\xi_p(t) v_p(t)||_2 \cdot \dfrac{f_p(t)}{||f_p(t)||_2} \qquad \text{otherwise.} \end{cases} \quad (12)$$

As can be seen in Eqs. (11) and (12), the variable excess of passivity is used in the design of a nonlinear controller

which scales down the force (a) when the energy cannot be absorbed by the patients' limb biomechanics, and (b) just enough to normalize the reflected force in the range which can be absorbed by the biomechanical passivity to satisfy the passivity condition and guarantee stability.

REFERENCES

[1] S. F. Atashzar *et al.*, "Haptics-enabled interactive neurorehabilitation mechatronics: classification, functionality, challenges and ongoing research," *Mechatronics*, vol. 57, pp. 1–19, 2019.

[2] C. Avraham and I. Nisky, "The effect of tactile augmentation on manipulation and grip force control during force-field adaptation," *Journal of NeuroEngineering and Rehabilitation*, vol. 17, no. 1, pp. 1–19, 2020.

[3] A. Milstein *et al.*, "Human-centered transparency of grasping via a robot-assisted minimally invasive surgery system," *IEEE Transactions on Human-Machine Systems*, vol. 48, no. 4, pp. 349–358, 2018.

[4] A. Jarc and I. Nisky, "Application and exploration of sensorimotor coordination strategies in surgical robotics," in *Metrics of Sensory Motor Coordination and Integration in Robots and Animals*. Springer, 2020, pp. 41–71.

[5] S. F. Atashzar *et al.*, "Haptic feedback manipulation during botulinum toxin injection therapy for focal hand dystonia patients: A possible new assistive strategy," *IEEE transactions on haptics*, vol. 9, no. 4, pp. 523–535, 2016.

[6] D. J. Reinkensmeyer *et al.*, "Computational neurorehabilitation: modeling plasticity and learning to predict recovery," *Journal of neuroengineering and rehabilitation*, vol. 13, no. 1, p. 42, 2016.

[7] J. Cao *et al.*, "Control strategies for effective robot assisted gait rehabilitation: the state of art and future prospects," *Medical engineering & physics*, vol. 36, no. 12, pp. 1555–1566, 2014.

[8] R. Sigrist *et al.*, "Augmented visual, auditory, haptic, and multimodal feedback in motor learning: a review," *Psychonomic bulletin & review*, vol. 20, no. 1, pp. 21–53, 2013.

[9] L. M. Crespo and D. J. Reinkensmeyer, "Review of control strategies for robotic movement training after neurologic injury," *Journal of neuroengineering and rehabilitation*, vol. 6, no. 1, p. 20, 2009.

[10] A. A. Blank *et al.*, "Current trends in robot-assisted upper-limb stroke rehabilitation: promoting patient engagement in therapy," *Current physical medicine and rehabilitation reports*, vol. 2, no. 3, pp. 184–195, 2014.

[11] R. Riener, "Robot-aided rehabilitation of neural function in the upper extremities," in *Operative Neuromodulation*. Springer, 2007, pp. 465–471.

[12] N. P. Fromme *et al.*, "Need for mechanically and ergonomically enhanced tremor-suppression orthoses for the upper limb: a systematic review," *Journal of neuroengineering and rehabilitation*, vol. 16, no. 1, p. 93, 2019.

[13] S. Shahtalebi *et al.*, "Phtnet: Characterization and deep mining of involuntary pathological hand tremor using recurrent neural network models," *Scientific Reports*, vol. 10, no. 1, pp. 1–19, 2020.

[14] S. F. Atashzar *et al.*, "Characterization of upper-limb pathological tremors: application to design of an augmented haptic rehabilitation system," *IEEE Journal of Selected Topics in Signal Processing*, vol. 10, no. 5, pp. 888–903, 2016.

[15] S. Shahtalebi *et al.*, "Wake: Wavelet decomposition coupled with adaptive kalman filtering for pathological tremor extraction," *Biomedical Signal Processing and Control*, vol. 48, pp. 179–188, 2019.

[16] Y. Zhou *et al.*, "Characterization of parkinsonian hand tremor and validation of a high-order tremor estimator," *IEEE Transactions on Neural Systems and Rehabilitation Engineering*, vol. 26, no. 9, pp. 1823–1834, 2018.

[17] N. Chopra *et al.*, "Bilateral teleoperation over unreliable communication networks," *IEEE Transactions on Control Systems Technology*, vol. 16, no. 2, pp. 304–313, 2008.

[18] M. Vidyasagar, *Nonlinear Systems Analysis*. SIAM, 2002, vol. 42.

[19] A. Aziminejad *et al.*, "Transparent time-delayed bilateral teleoperation using wave variables," *IEEE Transactions on Control Systems Technology*, vol. 16, no. 3, pp. 548–555, 2008.

[20] E. Nuno *et al.*, "A globally stable pd controller for bilateral teleoperators," *IEEE Trans. on Robotics*, vol. 24, no. 3, pp. 753–758, 2008.

[21] A. Jazayeri *et al.*, "Stability analysis of teleoperation systems under strictly passive and non-passive operator," in *World Haptics Conference*, April 2013, pp. 695–700.

[22] H. K. Khalil and J. Grizzle, *Nonlinear Systems*. Prentice hall, Upper Saddle River, 2002, vol. 3.

[23] C. A. Lawn and B. Hannaford, "Performance testing of passive communication and control in teleoperation with time delay," in *[1993] Proceedings IEEE International Conference on Robotics and Automation*. IEEE, 1993, pp. 776–783.

[24] M. Shahbazi *et al.*, "Position-force domain passivity of the human arm in telerobotic systems," *IEEE/ASME Transactions on Mechatronics*, vol. 23, no. 2, pp. 552–562, 2018.

[25] C. Yang *et al.*, "Teleoperation control based on combination of wave variable and neural networks," *IEEE Transactions on Systems, Man, and Cybernetics: Systems*, vol. 47, no. 8, pp. 2125–2136, 2016.

[26] K. Hashtrudi-Zaad and S. Salcudean, "Transparency in time-delayed systems and the effect of local force feedback for transparent teleoperation," *IEEE Tranactions on Robotics and Automation*, vol. 18, no. 1, pp. 108–114, 2002.

[27] G. Niemeyer and J.-J. E. Slotine, "Telemanipulation with time delays," *The International Journal of Robotics Research*, vol. 23, no. 9, pp. 873–890, 2004.

[28] V. Chawda and M. O'Malley, "Position synchronization in bilateral teleoperation under time-varying communication delays," *IEEE/ASME Trans. on Mechatronics*, vol. 20, no. 1, pp. 245–253, 2015.

[29] J. Zhang and C. C. Cheah, "Passivity and stability of human–robot interaction control for upper-limb rehabilitation robots," *IEEE Transactions on Robotics*, vol. 31, no. 2, pp. 233–245, 2015.

[30] J.-H. Ryu *et al.*, "Stability guaranteed control: Time domain passivity approach," *IEEE Transactions on Control Systems Technology*, vol. 12, no. 6, pp. 860–868, 2004.

[31] J.-H. Ryu *et al.*, "Time domain passivity control with reference energy following," *IEEE Transactions on Control Systems Technology*, vol. 13, no. 5, pp. 737–742, 2005.

[32] J.-H. Ryu *et al.*, "Stable teleoperation with time-domain passivity control," *IEEE Transactions on Robotics and Automation*, vol. 20, no. 2, pp. 365–373, 2004.

[33] S. F. Atashzar *et al.*, "A grasp-based passivity signature for haptics-enabled human-robot interaction: Application to design of a new safety mechanism for robotic rehabilitation," *The International Journal of Robotics Research*, vol. 36, no. 5-7, pp. 778–799, 2017.

[34] S. F. Atashzar *et al.*, "A small-gain approach for nonpassive bilateral telerobotic rehabilitation: Stability analysis and controller synthesis," *IEEE Transactions on Robotics*, vol. 33, no. 1, pp. 49–66, 2016.

[35] S. F. Atashzar *et al.*, "A passivity-based approach for stable patient–robot interaction in haptics-enabled rehabilitation systems: modulated time-domain passivity control," *IEEE Transactions on Control Systems Technology*, vol. 25, no. 3, pp. 991–1006, 2016.

[36] N. A. Tanner and G. Niemeyer, "High-frequency acceleration feedback in wave variable telerobotics," *IEEE/ASME Transactions on Mechatronics*, vol. 11, no. 2, pp. 119–127, 2006.

[37] M. Shahbazi *et al.*, "Networked dual-user teleoperation with time-varying authority adjustment: A wave variable approach," in *2014 IEEE/ASME International Conference on Advanced Intelligent Mechatronics*. IEEE, 2014, pp. 415–420.

[38] H. Lee and N. Hogan, "Energetic passivity of the human ankle joint," *IEEE Transactions on Neural Systems and Rehabilitation Engineering*, vol. 24, no. 12, pp. 1416–1425, 2016.

[39] H. Y. Huang *et al.*, "Cable-driven robotic interface for lower limb neuromechanics identification," *IEEE Transactions on Biomedical Engineering*, 2020. [Online]. Available: https://doi.org/10.1109/TBME.2020.3004491

[40] H. Y. Huang *et al.*, "The influence of posture, applied force and perturbation direction on hip joint viscoelasticity," *IEEE Transactions on Neural Systems and Rehabilitation Engineering*, vol. 28, no. 5, pp. 1138–1145, 2020.